SSNP171 - Closing of a crack in inflection

Summary

This test makes it possible to evaluate method XFEM with contact, during the closing of cracks.

One considers a test-tube 2D in inflection, comprising a central crack. The inflection of the test-tube causes a closing partial of the crack. On the bottom of crack remaining in opening, one test the stress intensity factor K_I. The theory provides that the taking into account of contact corrects the factor K_I of approximately 8%.

To measure the influence of the contact during closing, one plans seven modelings:

•Modeling a: a modeling 2D and of the linear elements, with interpenetration of the lips of the crack.

•Modeling B : a modeling 2D and of the linear elements, with contact between the lips of the crack.

•Modeling C: a modeling 2D and of the quadratic elements, with interpenetration of the lips of the crack.

•Modeling D : a modeling 2D and of the quadratic elements, with contact between the lips of the crack.

•Modeling E : a modeling 3D and of the linear elements, with interpenetration of the lips of the crack.

•Modeling F : a modeling 3D and of the linear elements, with contact between the lips of the crack.

•Modeling G : a modeling 3D and of the quadratic elements, with interpenetration of the lips of the crack.

1 Problem of reference

1.1 Geometry

The structure $2D$ is a rectangular test-tube ($LX=10$, $LY=20$), comprising a right and horizontal central crack [Figure 1.1-1]. The half-length of the crack is constant ($a=1$).

The structure 3D corresponds to an extrusion in direction Z of the test-tube 2D. The test-tube becomes parallelepipedic of dimensions : $LX=10$, $LY=20$, $LZ=1$. The crack length $a=1$ in the plan (X, Y) is also extruded according to Z.

Noted nodes $NOEUD1$, $NOEUD2$ on Figure 1.1-1 are used to impose the boundary conditions, which is clarified in the paragraph [§1.3].

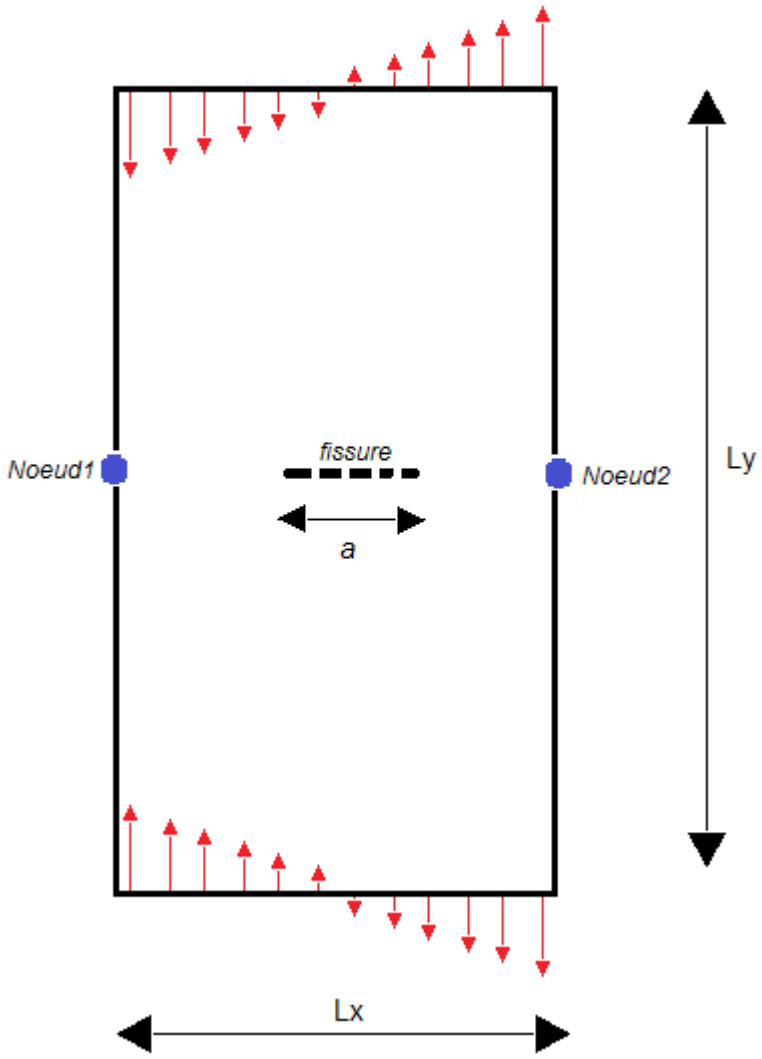

Figure 1.1-1: geometry of the fissured plate 2D

1.2 Properties of material

Young modulus: $E=10^6 Pa$

Poisson's ratio: $\nu = 0$
Density: $\rho = 7800\, kg/m^3$

1.3 Boundary conditions and loadings

Problem 2D (modelings A, B, C, D):

The loading consists in applying a density of linear force, left again to the edges inferior and superior of the test-tube [Figure 1.3-2].

To the higher edge one applies a density of force: $F_1(X, Y) = X$

To the lower edge one applies a density of force: $F_2(X, Y) = -X$

This loading exerts a compression on the half of test-tube (half on the left), a traction on other half of the test-tube (half on the right). It follows an inflection of the test-tube from there [Figure 3.4-1].

Thanks to this loading, one imposes:

•the closing of the crack, in the vicinity of the bottom of crack $P1 = (-a, 0)$, contained in half of the test-tube in compression;

•the opening of the crack, in the vicinity of the bottom of crack $P2 = (a, 0)$, contained in half of the tensile specimen (see [Figure 1.3-1])

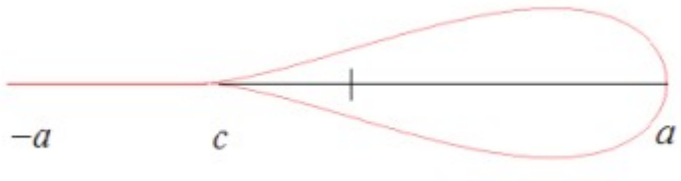

Figure 1.3-1: Partially closed crack

In order to block the rigid modes, displacements of the nodes are blocked $NOEUD1$, $NOEUD2$ as follows:

• $DX^1 = DY^1 = 0$

• $DY^2 = 0$.

This blocking is applied taking into account the field of displacement [Figure 3.4-1]. Indeed, displacement is rigorously null with the nodes considered, because they belong to the symmetry plane of the test-tube, around whose the test-tube bends.

3D problem (modelings E, F, G,):

The 3D problem takes again the whole of the limiting conditions of the problem 2D by adding only direction Z:
- efforts on Lface has superiorE $F_1(X, Y, Z) = X$,

- efforts on Lhas lower face $F_2(X, Y, Z) = -X$,

- the blocking of the rigid modes $DX^1=DY^1=DZ^1=0$, $DX^2=DY^2=0$ and one 3E not in the symmetry plane for the last rigid mode $DZ^3=0$.

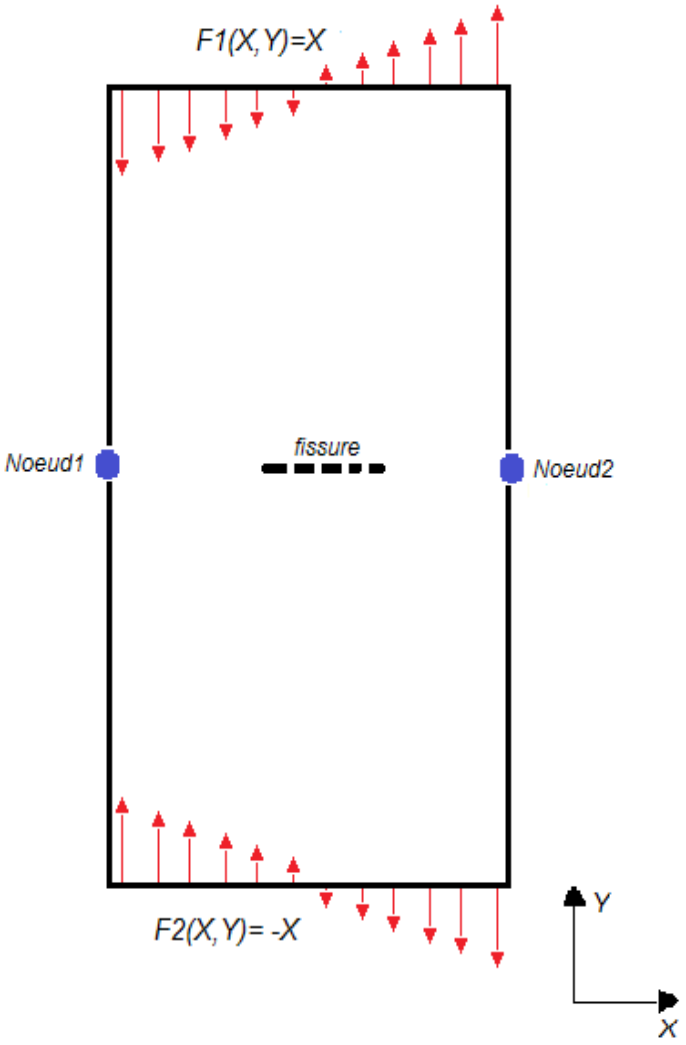

Figure 1.3-2: Limiting conditions problem 2D

2 Reference solution

2.1 Method of calculating

2.1.1 ModelingS WITH, C, E, G

One tests the stress intensity factor K_I compared to the analytical value without contact.

For a bend-test specimen and a right crack of X-coordinate $[-a\ ,\ a]$, the analytical value of K_I without closing of the crack, is determined by the formula of Bui [7] :

$$K_I=\frac{1}{\sqrt{\pi a}}\int_{-a}^{a} -t\sqrt{\frac{a-t}{t+a}}\,dt$$

where a indicate the half-length of the crack.

From the integral above, one calculates the expression simplified of K_I following:

$$K_I=\frac{a^{\frac{3}{2}}\sqrt{\pi}}{2}$$

Indeed in the integral, one carries out several changes of variables:

$t \rightarrow at$ one has $K_I=\frac{1}{\sqrt{\pi a}}a^2\int_{-1}^{1} -t\sqrt{\frac{1-t}{t+1}}\,dt$

$t\rightarrow t-1$ one has $K_I=\frac{1}{\sqrt{\pi a}}a^2\int_{0}^{2} -(t-1)\sqrt{\frac{2-t}{t}}\,dt$

$t\rightarrow 2t$ one has $K_I=\frac{1}{\sqrt{\pi a}}2a^2\int_{0}^{1} -(2t-1)\sqrt{\frac{1-t}{t}}\,dt$

$t \rightarrow t^2$ one has $K_I=\frac{1}{\sqrt{\pi a}}2a^2\int_{0}^{1} -2(2t^2-1)\sqrt{1-t^2}\,dt$

$t \rightarrow \sin t$ one has $K_I=\frac{1}{\sqrt{\pi a}}2a^2\int_{0}^{\frac{\pi}{2}} 2\cos 2t\cos^2 t\,dt$

After development of the product of $\cos$:

$$K_I=\frac{1}{\sqrt{\pi a}}2a^2\int_{0}^{\frac{\pi}{2}}\left(\frac{1}{2}+\cos 2t+\frac{1}{2}\cos 4t\right)dt$$

From where the final expression (after integration):

$$K_I=\frac{a^{\frac{3}{2}}\sqrt{\pi}}{2}$$

The half length being unit ($a=1$), one thus tests the stress intensity factor:

$$K_I=\frac{\sqrt{\pi}}{2}\approx 0,88629$$

By construction, there does not exist mode II. One thus tests: $K_{II}=0$

In addition, the rate of analytical refund of energy is worth:

$$G=\frac{1-\nu^2}{E}(K_I^2+K_{II}^2)\approx 7,853982\,E-7$$

2.1.2 Modeling B, D, F

For a bend-test specimen and a right crack of X-coordinate $[-a\ ,\ a]$, the analytical value of K_I with closing of the crack, is determined by the formula of Bui [7] :

$$K_I=\sqrt{\frac{2}{\pi(a-c)}}\int_c^a t\sqrt{\frac{t-c}{a-t}}\,dt$$

where c is the X-coordinate of the point for which the crack starts to open (see [Figure 1.3-1]) and a indicate the half-length of the crack.

One shows analytically [7] that the X-coordinate $c=-\frac{a}{3}$

Then, $K_I=\sqrt{\frac{3}{2\pi a}}\int_{-a/3}^a t\sqrt{\frac{t+a/3}{a-t}}\,dt$

From the integral above, one calculates the expression simplified of K_I following:

$$K_I=(\frac{2}{3}a)^{\frac{3}{2}}\sqrt{(\pi)}$$

Indeed in the integral, one carries out several changes of variables:

$t\rightarrow at$ one has $K_I=\sqrt{\frac{3}{2\pi a}}a^2\int_{-1/3}^1 t\sqrt{\frac{t+1/3}{1-t}}\,dt$

$t\rightarrow t-\frac{1}{3}$ one has $K_I=\sqrt{\frac{3}{2\pi a}}a^2\int_0^{4/3}(t-\frac{1}{3})\sqrt{\frac{t}{4/3-t}}\,dt$

$t\rightarrow \frac{4}{3}t$ one has $K_I=\sqrt{\frac{3}{2\pi a}}a^2\frac{4}{9}\int_0^1(4t-1)\sqrt{\frac{t}{1-t}}\,dt$

$t\rightarrow t^2$ one has $K_I=\sqrt{\frac{3}{2\pi a}}a^2\frac{4}{9}\int_0^1(4t^2-1)\frac{2t^2}{\sqrt{1-t^2}}\,dt$

$t\rightarrow \sin t$ one has $K_I=\sqrt{\frac{3}{2\pi a}}a^2\frac{4}{9}\int_0^{\pi/2}(4\sin^2 t-1)(2\sin^2 t)\,dt$

After development of the powers of $\sin t$:

$$K_I=\sqrt{\frac{3}{2\pi a}}a^2\frac{4}{9}\int_0^{\pi/2}(2-3\cos 2t+\cos 4t)\,dt$$

From where the final expression (after integration):

$$K_I=(\frac{2}{3}a)^{\frac{3}{2}}\sqrt{(\pi)}$$

The half length being unit ($a=1$), one thus tests the stress intensity factor:

$$K_I=(\frac{2}{3})^{\frac{3}{2}}\sqrt{(\pi)}\approx 0,9648017$$

By construction, there does not exist mode II. One thus tests: $K_{II}=0$

In addition, the rate of analytical refund of energy is worth:

$$G=\frac{1-\nu^2}{E}(K_I^2+K_{II}^2)\approx 9,308423\,E-7$$

2.2 Sizes and results of reference

One tests K_I , K_{II} and G .

2.2.1 Modelings A, C, E, F, G

$$K_I=\frac{\sqrt{\pi}}{2}\approx 0,88629$$
$$K_{II}=0$$
$$G=\frac{1-\nu^2}{E}(K_I^2+K_{II}^2)\approx 7,853982\,E-7$$

2.2.2 Modeling B and D

$$K_I=(\frac{2}{3})^{\frac{3}{2}}\sqrt{(\pi)}\approx 0,9648017$$
$$K_{II}=0$$
$$G=\frac{1-\nu^2}{E}(K_I^2+K_{II}^2)\approx 9,308423\,E-7$$

2.3 Uncertainty on the solution

Weak, semi-analytical solution.

2.4 Bibliographical references

[1] GENIAUT S., MASSIN P.: eXtended Finite Method Element, Handbook of reference of *Code_Aster*, [R7.02.12]

[2] GENIAUT S.: Approach XFEM for cracking under contact of industrial structures, Doctorate GeM Laboratory, 2006.

[3] H.D. DrunkI: Breaking process fragile, ED. Masson, 1978.

[4] THRESHER R.W., SMITH F.W.: The partially closed Griffith ace, *International Newspaper of Fracture* , vol. 9, n°1, pp. 33-41, 1973

[5] Rice, J.R. (1968), “with path independent integral and the approximate analysis of strain concentration by notches and aces”, *Newspaper of Applied Mechanics* **35** : 379-386

3 Modeling A

3.1 Characteristics of modeling

In this modeling, wide finite element method (X-FEM) is used. The finite elements are linear.
A ray of enrichment is defined elements X-FEM melts of crack $R_{ENRI}=0.5$. This ray of enrichment makes it possible more precisely to collect the singular asymptotic solution in bottom of crack. Relatively broad size of ray (25 % length of the crack) does not introduce problem of conditioning, taking into account the new approximation in bottom of crack [R7.02.12].

3.2 Characteristics of the grid

One refines the grid in the center of the test-tube, in order to optimize the calculation of the solution in displacement in the vicinity of the crack [Figure 3.2-1].

```
MANY NODES                    4088
MANY MESHS                    4360
                    SEG2                    80
                    TRIA3                  466
                    QUAD4                 3814
```

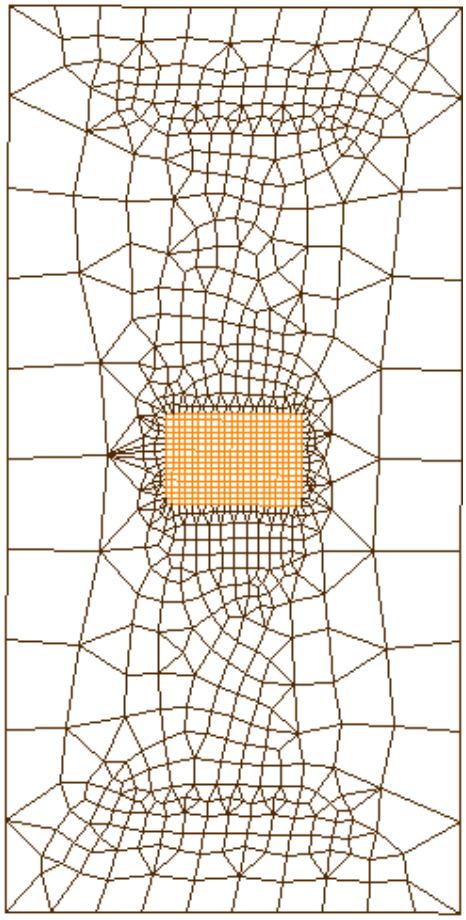

Figure 3.2-1: Grid of the field

3.3 Sizes tested and results

On the bottom of crack in opening $P2=(a,0)$, one tests the stress intensity factor K_I given by the order CALC_G, compared to the analytical value clarified in the paragraph [5].

For the method $G-thêta$ (order CALC_G), L is chosenbe crownS field theta followingS :

	Crown 1	Crown 2	Crown 3	Crown 4	Crown 5	Crown 6
Rinf	0.1	0.2	0.3	0.1	0.1	0.2
Rsup	0.2	0.3	0.4	0.3	0.4	0.4

Identification	Type of reference	Value of Référence	Precision
CALC_G/K1	'ANALYTICAL'	0.88629	1.0%
CALC_G/K2	'ANALYTICAL'	0,00	0.001%
CALC_G/G	'ANALYTICAL'	7.85514E-07	2.0%

3.4 Complementary results

Here the field of displacement calculated by Aster, without activating algorithm of contact between the lips of crack:

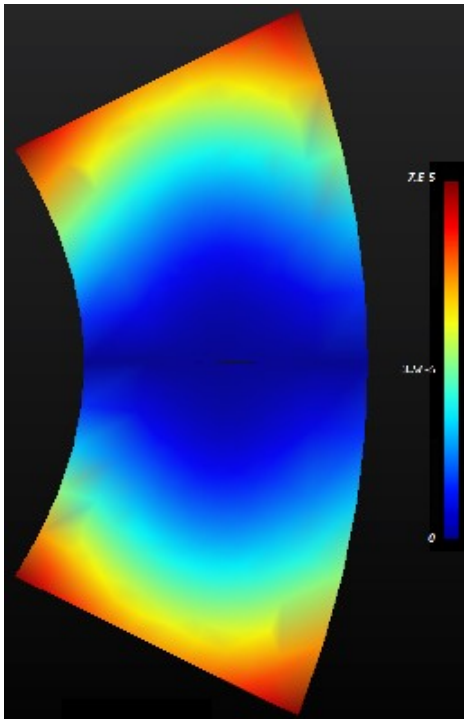

Figure 3.4-1: Field of displacement (with offset)

4 Modeling B

4.1 Characteristics of modeling

In this modeling, wide finite element method (X-FEM) is used. A ray of enrichment is defined $R_{ENRI}=0.5$. The finite elements are linear.

4.2 Characteristics of the grid

Identical to modeling A.

4.3 Sizes tested and results

On the bottom of crack in opening $P2=(a,0)$, one tests the stress intensity factor K_I given by the order CALC_G, compared to the analytical value clarified in the paragraph [5].

For the method $G-thêta$ (order CALC_G), L is chosenbe crownS field theta followingS :

	Crown 1	Crown 2	Crown 3	Crown 4	Crown 5	Crown 6
Rinf	0.1	0.2	0.3	0.1	0.1	0.2
Rsup	0.2	0.3	0.4	0.3	0.4	0.4

Identification	Type of reference	Value of Référence	Precision
CALC_G/K1	'ANALYTICAL'	0.9648	1.0 %
CALC_G/K2	'ANALYTICAL'	0,00	0.001
CALC_G/G	'ANALYTICAL'	9,3084E-7	2.0%

4.4 Complementary results

By activating the algorithm of contact, one obtains the solution in displacement in the vicinity of the crack given to [Figure 1.3-1] (to be compared with postprocessing Figure 4.4-1).

In addition, one finds an analytical conclusion, namely the X-coordinate of the point for which the crack starts to open:

$$c=-\frac{a}{3}\approx-0.33$$

Indeed, in postprocessing, we analyzed contact pressures to determine the X-coordinate of the last point of contact. Graphically, it is estimated that the pressure falls fo rtement around the point of X-coordinate $x_c\approx-0.325$, what validates the assumption of estimate of K_I .

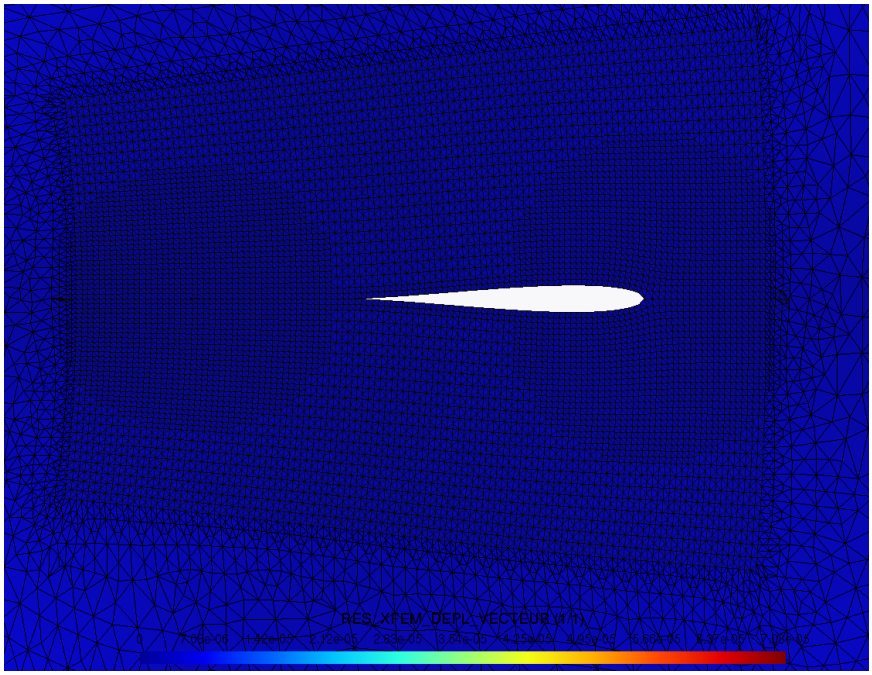

Figure 4.4-1 : facies of closing of the crack with contact

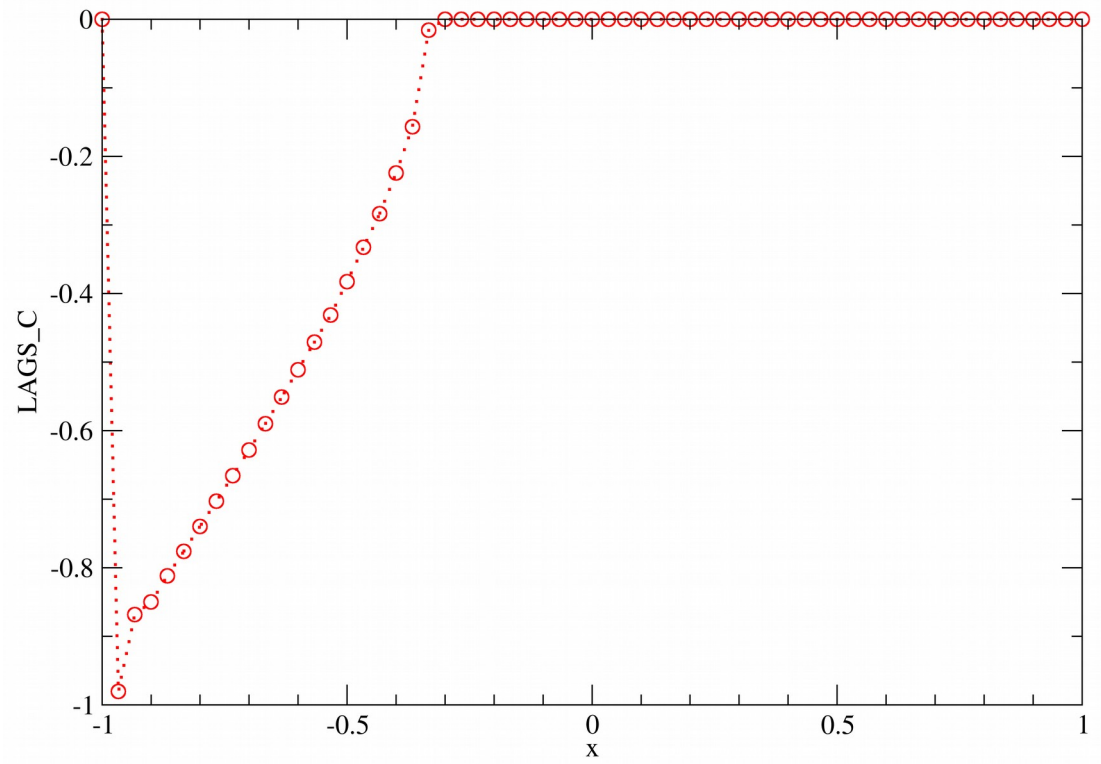

Figure 4.4-2: contact pressure along the crack

5 Modeling C

5.1 Characteristics of modeling

Identical to modeling A with quadratic elements.

5.2 Characteristics of the grid

```
MANY NODES                      12455

MANY MESHS                      4360
                              SEG3                80
                              TRIA6              466
                              QUAD8             3814
```

5.3 Sizes tested and results

For the method $G-thêta$ (order CALC_G), L is chosenbe crownS field theta followingS :

	Crown 1	Crown 2	Crown 3	Crown 4	Crown 5	Crown 6
Rinf	0.1	0.2	0.3	0.1	0.1	0.2
Rsup	0.2	0.3	0.4	0.3	0.4	0.4

Identification	Type of reference	Value of Référence	Precision
CALC_G/K1	'ANALYTICAL'	0.88629	0.05%
CALC_G/K2	'ANALYTICAL'	0,00	0.001
CALC_G/G	'ANALYTICAL'	7.85514E-07	1, 0%

5.4 Comments

The results are more precise than modeling A.

6 Modeling D

6.1 Characteristics of modeling

Identical to modeling B with quadratic elements.

6.2 Characteristics of the grid

Identical with modeling C.

6.3 Sizes tested and results

For the method $G-thêta$ (order CALC_G), L is chosenbe crownS field theta followingS :

	Crown 1	Crown 2	Crown 3	Crown 4	Crown 5	Crown 6
Rinf	0.1	0.2	0.3	0.1	0.1	0.2
Rsup	0.2	0.3	0.4	0.3	0.4	0.4

Identification	Type of reference	Value of Référence	Precision
CALC_G/K1	'ANALYTICAL'	0.9648	1.0 %
CALC_G/K2	'ANALYTICAL'	0,00	0.01
CALC_G/G	'ANALYTICAL'	9,3084E-7	2.0%

6.4 Comments

With the quadratic elements one does not note profit by activating the algorithm of contact compared to the linear elements (modeling B). The singularity at the point of separation could generate a poor convergence of the algorithm of contact (the space of the multipliers collects with difficulty the singularity of the stress field at the point of separation, cf. Figure 4.4-2), which would generate a difficulty of collecting the solution expected for this physical problem.

Nevertheless the results are very satisfactory being given the weak refinement of the grid (less than 1500 elements).

7 Modeling E

7.1 Characteristics of modeling

Extrusion of modeling A with elements linear.

7.2 Characteristics of the grid

```
MANY NODES                          3868

MANY MESHS                          3240
                                  QUAD4                  120
                                  PENTA6                 564
                                  HEXA8                 2556
```

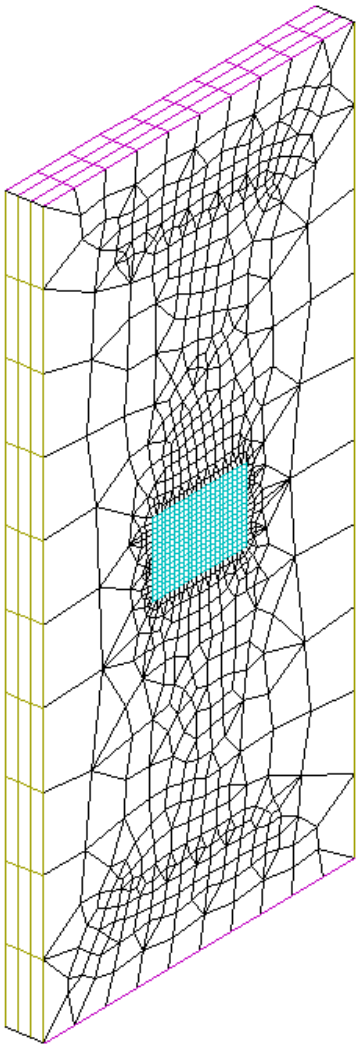

Figure 7.2-1 : Grid with central zone refined in HEXA20

7.3 Sizes tested and results

For the method $G-thêta$ (order CALC_G), L is chosenbe crownS field theta followingS :

	Crown 1	Crown 2	Crown 3	Crown 4	Crown 5	Crown 6

Rinf	0.1	0.2	0.3	0.1	0.1	0.2
Rsup	0.2	0.3	0.4	0.3	0.4	0.4

Identification	Type of reference	Value of Référence	Precision
CALC_G/K1 (MAX)	'ANALYTICAL'	0.88629	2,0%
CALC_G/K1 (MIN)	'ANALYTICAL'	0.88629	2,0%
CALC_G/K2 (MAX)	'ANALYTICAL'	0,00	0.004
CALC_G/K2 (MIN)	'ANALYTICAL'	0,00	0.004
CALC_G/G (MAX)	'ANALYTICAL'	7.85514E-07	4, 0%
CALC_G/G (MIN)	'ANALYTICAL'	7.85514E-07	4, 0%

7.4 Comments

In 3D, one notes a light degradation of the precision for the calculation of the factors compared to an equivalent modeling 2D (modeling A).

8 Modeling F

Extrusion of modeling B with elements linear.

8.1 Characteristics of the grid

Identical to modeling E.

8.2 Sizes tested and results

For the method $G-thêta$ (order CALC_G), L is chosenbe crownS field theta followingS :

	Crown 1	Crown 2	Crown 3	Crown 4	Crown 5	Crown 6
Rinf	0.1	0.2	0.3	0.1	0.1	0.2
Rsup	0.2	0.3	0.4	0.3	0.4	0.4

Identification	Type of reference	Value of Référence	Precision
CALC_G/K1 (MAX)	'ANALYTICAL'	0.9648	2,0%
CALC_G/K1 (MIN)	'ANALYTICAL'	0.9648	2,0%
CALC_G/K2 (MAX)	'ANALYTICAL'	0,00	0.004
CALC_G/K2 (MIN)	'ANALYTICAL'	0,00	0.004
CALC_G/G (MAX)	'ANALYTICAL'	9,3084E-7	4, 0%
CALC_G/G (MIN)	'ANALYTICAL'	9,3084E-7	4, 0%

8.3 Comments

In 3D, one notes a light degradation of the precision for the calculation of the factors compared to an equivalent modeling 2D (modeling B).

9 Modeling G

Extrusion of modeling With with elements quadratic.

9.1 Characteristics of the grid

```
MANY NODES                    14793

MANY MESHS                    3240
                            QUAD8              120
                            PENTA15            564
                            HEXA20            2556
```

9.2 Sizes tested and results

For the method $G-thêta$ (order CALC_G), L is chosenbe crownS field theta followingS :

	Crown 1	Crown 2	Crown 3	Crown 4	Crown 5	Crown 6
Rinf	0.1	0.2	0.3	0.1	0.1	0.2
Rsup	0.2	0.3	0.4	0.3	0.4	0.4

Identification	Type of reference	Value of Référence	Precision
CALC_G/K1 (MAX)	'ANALYTICAL'	0.88629	0.5%
CALC_G/K1 (MIN)	'ANALYTICAL'	0.88629	0.5%
CALC_G/K2 (MAX)	'ANALYTICAL'	0,00	0.001
CALC_G/K2 (MIN)	'ANALYTICAL'	0,00	0.001
CALC_G/G (MAX)	'ANALYTICAL'	7.85514E-07	1, 0%
CALC_G/G (MIN)	'ANALYTICAL'	7.85514E-07	1, 0%

9.3 Comments

In 3D, one notes an improvement of the results compared to modeling with the linear elements (modeling E).

10 Summaries of the results

During the closing of a crack, the taking into account of the contact between the lips significantly affect the stress intensity factor K_I, compared to method XFEM without contact.

In this CAS-test, one finds a difference about 8% on the value of K_I calculated by Aster, while passing from modeling A (without contact between the lips) to modeling B (with contact). This difference is in agreement with the theoretical forecasts.

Indeed, the theory provides that the difference is worth:

$$\frac{K_I^{\text{avec contact}} - K_I^{\text{sans contact}}}{K_I^{\text{avec contact}}} = \frac{\left((2/3)^{\frac{3}{2}} - 1/2\right)}{(2/3)^{\frac{3}{2}}} \approx 8{,}14413\%$$

The got results show that the value of K_I with taking into account of the contact is well correctly evaluated and higher than that obtained without taking into account of the contact. This result stresses the importance of the taking into account of the effects related to the contact in the digital simulations of cracking, because this example illustrates a case where the solution with interpenetration (without contact) is not conservative from the point of view of the stress intensity factors. That can prove not without consequence for the study of the propagation, based on criteria of propagation written according to the stress intensity factors.